



THE UNIVERSITY *of* EDINBURGH

Edinburgh Research Explorer

Impact of sea-ice melt on dimethyl sulfide (sulfoniopropionate) inventories in surface waters of Marguerite Bay, West Antarctic Peninsula

Citation for published version:

Stefels, J, Van Leeuwe, MA, Jones, EM, Meredith, MP, Venables, HJ, Webb, AL & Henley, SF 2018, 'Impact of sea-ice melt on dimethyl sulfide (sulfoniopropionate) inventories in surface waters of Marguerite Bay, West Antarctic Peninsula', *Philosophical Transactions A: Mathematical, Physical and Engineering Sciences*, vol. 376, no. 2122, pp. 20170169. <https://doi.org/10.1098/rsta.2017.0169>

Digital Object Identifier (DOI):

[10.1098/rsta.2017.0169](https://doi.org/10.1098/rsta.2017.0169)

Link:

[Link to publication record in Edinburgh Research Explorer](#)

Document Version:

Peer reviewed version

Published In:

Philosophical Transactions A: Mathematical, Physical and Engineering Sciences

General rights

Copyright for the publications made accessible via the Edinburgh Research Explorer is retained by the author(s) and / or other copyright owners and it is a condition of accessing these publications that users recognise and abide by the legal requirements associated with these rights.

Take down policy

The University of Edinburgh has made every reasonable effort to ensure that Edinburgh Research Explorer content complies with UK legislation. If you believe that the public display of this file breaches copyright please contact openaccess@ed.ac.uk providing details, and we will remove access to the work immediately and investigate your claim.



Impact of sea-ice melt on DMS(P) inventories in surface waters of Marguerite Bay, West-Antarctic Peninsula.

Journal:	<i>Philosophical Transactions A</i>
Manuscript ID	RSTA-2017-0169.R1
Article Type:	Research
Date Submitted by the Author:	n/a
Complete List of Authors:	Stefels, Jacqueline; Rijksuniversiteit Groningen Faculteit voor Wiskunde en Natuurwetenschappen, GELIFES van Leeuwe, Maria; Rijksuniversiteit Groningen Faculteit voor Wiskunde en Natuurwetenschappen, GELIFES Jones, Elizabeth; Institute of Marine Research Meredith, Michael; British Antarctic Survey, Venables, Hugh; British Antarctic Survey, Webb, Alison; Rijksuniversiteit Groningen Faculteit voor Wiskunde en Natuurwetenschappen, GELIFES Henley, Sian; University of Edinburgh School of GeoSciences, School of GeoSciences
Issue Code (this should have already been entered but please contact the Editorial Office if it is not present):	WAP
Subject:	Oceanography < EARTH SCIENCES, Biogeochemistry < EARTH SCIENCES
Keywords:	DMS, DMSP, sea ice, phytoplankton community structure, Haptophytes, west Antarctic Peninsula

SCHOLARONE™
Manuscripts

Impact of sea-ice melt on DMS(P) inventories in surface waters of Marguerite Bay, West-Antarctic Peninsula.

Jacqueline Stefels^{1,a}, Maria A. van Leeuwe¹, Elizabeth M. Jones^{2,b}, Michael P. Meredith³, Hugh J. Venables³, Alison L. Webb¹, Sian F. Henley⁴

1. University of Groningen, Groningen Institute for Evolutionary Life Sciences, Nijenborgh 7, 9747 AG Groningen, The Netherlands

2. University of Groningen, Center for Energy and Environmental Sciences, Nijenborgh 6, 9747 AG Groningen, The Netherlands

3. British Antarctic Survey, High Cross, Madingley Road, Cambridge, CB3 0ET, UK

4. School of GeoSciences, University of Edinburgh, James Hutton Road, Edinburgh, EH9 3FE, UK

a. Corresponding author: j.stefels@rug.nl

b. Current institution: Institute of Marine Research, Postboks 6606 Langnes, 9296 Tromsø, Norway

Abstract

The Southern Ocean is a hotspot of the climate-relevant organic sulphur compound dimethyl sulphide (DMS). Spatial and temporal variability in DMS concentration is higher than in any other oceanic region, especially in the marginal ice zone. During a one-week expedition across the continental shelf of the west Antarctic Peninsula (WAP), from the shelf break into Marguerite Bay, in January 2015, spatial heterogeneity of DMS and its precursor dimethyl sulphoniopropionate (DMSP) was studied and linked with environmental conditions, including sea ice melt events. Concentrations of sulphur compounds, particulate organic carbon (POC) and chlorophyll *a* in the surface waters varied by a factor of 5 to 6 over the entire transect. DMS and DMSP concentrations were an order of magnitude higher than currently inferred in climatologies for the WAP region. Particulate DMSP (DMSPp) concentrations were correlated most strongly with POC and the abundance of Haptophyte algae within the phytoplankton community, which in turn was linked with sea-ice melt. The strong sea-ice signal in the distribution of DMS(P) implies that DMS(P) production is likely to decrease with ongoing reductions in sea ice cover along the WAP. This has implications for feedback processes on the region's climate system.

Keywords:

DMS, DMSP, sea ice, phytoplankton community structure, Haptophytes, west Antarctic Peninsula

42 Introduction

43 The semi-volatile organic sulphur compound dimethyl sulphide (DMS) is the most important natural
44 sulphur source to the atmosphere, where it forms an important precursor of aerosols after oxidation
45 to sulphate. Oceans are the main source of DMS, contributing >90% to the global flux. The modelled
46 contribution of DMS to the climate-relevant non-sea-salt sulphate (nss-SO_4^{2-}) is especially high in the
47 Southern Ocean, where human impacts are smallest, with a mean annual contribution of 43% to
48 Southern Hemisphere nss-SO_4^{2-} and an 85% contribution to nss-SO_4^{2-} over the summer period ((1)).
49 Aerosols and clouds contribute to the albedo of the atmosphere. This has led to the well-known
50 CLAW hypothesis, whereby a negative feedback exists between the production of DMS in the ocean
51 and the albedo of the sky and clouds, thus regulating Earth's climate (2). Although this hypothesis
52 inspired much research, there are still large uncertainties about many aspects of the hypothesis,
53 especially in remote locations like the Southern Ocean.

54 Modelling the radiation budget around Antarctica is one of the biggest uncertainties in projections of
55 global climate. This is at least partly due to the fact that oxidation pathways in the atmosphere are
56 intrinsically complex with large impacts on the efficiency of the DMS-to- SO_4^{2-} pathway (3).
57 Nonetheless, high numbers of ultra-fine particles have been observed in air masses coming from
58 Antarctic sea-ice areas and it has been suggested that DMS is a potential source (4). Indeed, high
59 DMS fluxes have been found above sea ice, but it remains unclear how much can be attributed to
60 direct flux from surface communities in ice, or from leads between ice floes where surface-
61 microlayer concentrations of DMS are typically 10-fold higher than in the underlying water column
62 (5)(6). So far, most attention has been paid to the impact of changing sea-ice cover on the pelagic
63 ecosystem and its consequences for DMS release. Coupled climate simulations have shown a 150%
64 increase in zonal-averaged DMS flux in the Southern Ocean, when modelling a future world with an
65 atmospheric CO_2 concentration of 970 ppm. This increase is due to sea-ice reductions and concurrent
66 ocean community changes, and did not involve DMS flux from sea ice itself (7).

67 Climatologies of DMS concentrations and fluxes to the atmosphere show that the Southern Ocean as
68 a whole is a global hot spot of DMS production (8). A recent update of the Southern Ocean summer-
69 time climatology of DMS confirms the region's importance and calculates an overall increase in
70 concentrations and fluxes compared to Lana et al. (9). The Southern Ocean is also the region with
71 highest temporal variability in DMS concentrations, whereby highest concentrations are observed in
72 the Marginal Ice Zone (MIZ). Data from the West Antarctic Peninsula (WAP) region are scarce, with
73 only a few published datasets (10) (9) (11). Two time-series from the Palmer Long-Term Ecological
74 Research (LTER) program show increasing DMS concentrations in December, reaching relatively
75 stable concentrations in January between 5 and 15 nM and an occasional maximum exceeding 25 nM
76 (10) (11). A recent multi-year time series at the Rothera Time-Series (RaTS) site in northern
77 Marguerite Bay, shows a similar pattern, but with much higher concentrations. Here, DMS
78 concentrations exceeded 20 nM during several weeks in January of each year, with a maximum of
79 160 nM in January 2015 (Webb et al. in prep).

80 The cause of the difference between the Palmer LTER and RaTS datasets is yet unexplained, but we
81 hypothesise an important role for sea ice in modulating the magnitude of DMS concentrations. Sea-
82 ice conditions along the WAP have changed dramatically since the onset of the satellite era in the
83 late 1970s, resulting in an increase in the length of the summer ice-free season by more than 3
84 months (12). These changes are strongest in the northern part of the WAP, where sea ice losses have
85 been significantly more pronounced than further south and in the Marguerite Bay region (13).
86 Impacts of these changes on the ecosystem are now becoming apparent, with strong reductions in
87 primary production in the northern part of the WAP and increased primary production in the
88 southern WAP region (14). Average sea-ice coverage over the last 5 years shows that the northern
89 boundary of the retreating MIZ at Palmer occurs two months earlier than at Rothera (Figure 1a and
90 b), with potential consequences for the timing and magnitude of the phytoplankton bloom. The
91 impact of sea ice on primary production acts through stabilization of the upper mixed layer, thereby
92 offering favourable conditions for phytoplankton growth (15), but also potentially through seeding

algae to the surface waters when high algal biomass is released upon ice melt (16) (17). The consequences of sea ice changes for DMS(P) production are yet unknown.

Large blooms and spikes of DMS in the MIZ have been associated with melting ice (18). These DMS spikes may be caused by the release upon ice melt of large amounts of ice algae that produce the precursor of DMS, dimethyl sulphoniopropionate (DMSP). DMSP is an important osmolyte for ice algae (19). As a result, extremely high DMSP concentrations in sea ice – two to three orders of magnitude higher than in the underlying surface waters (20) – are a common feature. When sea ice decays, ice algae are released to the water column, and this may result in a release of DMSP from the cells and subsequent enzymatic conversion into DMS. Direct evidence for this pathway is limited, however, and a large range of water-column inventories of DMS have been observed in different studies in the MIZ. For instance, in a time-series study in the Weddell Sea in which both sea ice and surface water were monitored simultaneously, the loss of two-thirds of the DMSP inventory in sea ice co-occurred with increases of DMSP in the water column, but only a small increase in DMS, with concentrations around 1 nM (20).

The role of sea ice in the flux of DMS to the atmosphere is complex and we are far from having a quantitative understanding of the processes involved. The efficiency with which DMSP is converted to DMS strongly depends on the community structure of the microbial foodweb (21), in combination with abiotic factors such as salinity, temperature, nutrient availability and light conditions (22). High salinity, low temperature, nutrient limitation and high-light stress in sea-ice ecosystems may all result in increased production of DMSP, especially by the well-known DMSP producer *Phaeocystis antarctica*, which is often found in surface-ice communities (20). Upon ice melt, brine channels open and surface communities are flushed. Reductions in salinity, increased temperatures and potential invasion of the brine channels by zooplankton that graze on ice algae are processes with the potential to release DMSP from algal cells. Subsequent conversion to DMS depends both on the algal and bacterial community composition, because *Phaeocystis* and dinoflagellates can have an active DMSP-lyase enzyme that converts DMSP into DMS, whereas diatoms do not (22). In addition, an active bacterial community can add to the DMSP cleavage into DMS, but also use DMSP as a carbon and sulphur source, thereby diverting DMSP consumption away from DMS production (22).

The latest DMS climatology of the Southern Ocean does not indicate that the WAP is a particularly profound hotspot of DMS production (9); however, this may at least partly be due to a lack of data within the marginal ice zone. These authors make a case for using a summer-time climatology, covering the December through February months in a single data point, which results in a calculated DMS concentration for the WAP of around 10 nM. Although this approach may be justified on a basin scale when a limited number of data points are available, it does not account for the large and dynamic fluctuations we observed during time-series measurements in Marguerite Bay (Webb et al. in prep.), and may inadvertently dampen climatologically-important fluxes. The objective of the current project was to study the spatial heterogeneity of DMS(P) concentrations in the upper ocean across the WAP shelf, from the shelf break to Marguerite Bay, including the RaTS site. Through linking the concentrations of these compounds with environmental conditions, including sea ice melt-water inputs, we obtain a better understanding of the ecological factors that drive the demonstrated heterogeneity and study the relative contribution of DMS(P) released from sea ice to the pelagic environment. This is important knowledge that is needed to improve our understanding on the impact of interannual variability and potential long-term trends in sea-ice growth and retreat on the regional production of DMS and ultimately on global climate.

137
138 **Materials & Methods**

139 *Sampling*

140 This study was conducted on board RRS James Clark Ross during the JR307 cruise. For a full
141 description of sampling see Henley et al. (this issue)(23). In brief: From 1 to 7 January 2015, 11
142 profiles were taken along a cruise track that followed Marguerite Trough from the shelf break
143 (station T01) into Ryder Bay (station T10, which coincides with the location of the RaTS site) (Figure

1c). At each station, a full-depth conductivity-temperature-depth (CTD) cast was taken with a Seabird SBE911Plus package attached to a 24-bottle rosette frame. Water samples were taken at each station on the upcast of CTD deployments from 12 L Niskin bottles. One set of bottles was sampled over the full depth for carbonate system parameters, macronutrients, oxygen isotopes of seawater and salinity (23).

In addition to these parameters, 6 Niskin bottles were used to sample the upper 120 m for total and filtered fractions of DMS + DMSP, particulate organic carbon (POC) concentrations and $\delta^{13}\text{C}$ -POC, and phytoplankton pigments. Samples were taken from various depths: 5, 15, 25, 40, 70 and 100 or 120m depending on the depth of the pycnocline. First, duplicate 70 mL samples for DMS(P)-compounds were collected in amber-glass vials, using silicone tubing from the Niskin nozzle. Care was taken that no bubbles formed in the tubing and that the vials were superfluously overflowed with sample water before carefully removing the tubing. The vials were closed with screw caps containing teflon-faced liners. Secondly, a 0.5L teflon bottle was filled for POC samples and an additional 4.5L polycarbonate Nalgene bottle for phytoplankton pigments. Before sampling, all sample bottles were thoroughly rinsed with Milli-Q water and the sample water. After collection, samples were stored in the dark and cold and immediately processed on board.

Chemical analyses

S-compounds

From each 70 mL sample a 10 mL subsample was transferred to a 20 mL vial; 1 pellet of NaOH (approximately 0.2g) was added to convert all DMSP to DMS and the vial was closed with a teflon-coated crimp cap. This sample contains all DMS and dissolved and particulate DMSP (DMSPd and DMSPp respectively) and is denoted as DMS(P)t. The remainder of the sample was gently poured into a Sartorius filter holder containing a 4.5cm Whatmann GF/F filter and filtered using gravity filtration only, thereby making sure that the filter holder was removed from the filtrate well before the filter would run dry in order to prevent release of DMSP from algal cells. From approximately 20 mL of filtrate, one 10 mL subsample was taken and stored in 20 mL vials; 1 pellet of NaOH was added and the vial was closed with a teflon-coated crimp cap. This sample contains all DMS and DMSPd and is denoted DMS(P)d. All samples were kept at $\sim 15^\circ\text{C}$ in the lab. Samples were analysed upon return to Rothera Research Station in the week after the cruise had taken place.

DMS was analysed on a Proton-Transfer Reaction Time-Of-Flight Mass Spectrometer (PTR-TOF8000, IONICON GmbH, Innsbruck, Austria). The time-of-flight analyser was set to analyse a mass-to-charge (m/z) range from 0 to 256 at a sampling rate of 25 kHz. Data were averaged over 1.2 sec intervals. An advantage of the PTR-TOFMS is that most proton transfer processes are non-dissociative, so that the compounds are not fragmented during ionization. As a consequence, there is only one protonated product to be analysed. Hence, the compound of interest is analysed as its mass plus one: in the case of DMS as mass 63.

Flow rates of carrier gas through the sample and into the PTR-TOFMS were kept constant by the instrument's pressure regulators: total input flow rate is set to 150 mL/min, whereas the rate into the instrument's drift tube is ~ 10 mL/min, which is maintained at a constant pressure of 2.2 hPa. Lab air is used as carrier gas after cleaning with a zero-air generator (Parker-Balston). DMS(P) samples were analysed directly by putting the 20 mL vials in-line with the inlet flow, using two needles through the vial's stopper. When attaching a sample, DMS is swept out of the vial, via an overflow vial, into the PTR-TOFMS, resulting in an exponentially decaying peak. Depending on the amount of DMS in the sample, the signal came back to base-line levels after 6 to 15 minutes. Total amounts were calculated by integration of peak areas. Daily, a $\sim 6\ \mu\text{M}$ DMS working standard was prepared in Milli-Q water from a primary $\sim 60\text{mM}$ DMS standard, prepared from pure DMS (Sigma-Aldrich) in methanol. From the working standard, standards of $\sim 30\ \text{nM}$ were analysed regularly in between the samples. Standard curves proved to be linear over more than 3 orders of magnitude, with typical correlation coefficients larger than 0.999 when using 8 concentration steps and a detection limit of 1 pmol DMS per sample.

1
2 195 Particulate DMSP (DMSPp) was calculated after subtracting DMS(P)d from DMS(P)t. The DMS(P)d
3 196 concentrations provide an upper limit to the potential concentration of DMS. During two surveys in
4 197 the nearby Ryder Bay, also in January 2015, for which it was possible to analyse both DMS and
5 198 DMSPd separately, the fraction of DMS within the DMS(P)d pool reached 84 and 93% respectively
6 199 (n=13 and 17). In discussing our data, we used a conservative estimate of 80% to calculate the DMS
7 200 contribution.
8
9 201
10 202 POC
11
12 203 Samples for POC analysis were collected through gentle filtering (<15 KPa) of the 0.5L sample over
13 204 2.5 cm pre-combusted Whatman GF/F filters. Filters were snap-frozen in liquid nitrogen, wrapped in
14 205 aluminium foil and stored at -20°C until analysis at the home laboratory. To remove inorganic carbon,
15 206 the filters were left in an exicator with 4 ml 37% fuming HCL for 4 hours and dried at 60°C overnight.
16 207 Before analysis, filters were packed in 5x12 mm tin cups. Samples were analysed with a combustion
17 208 module attached to a Cavity Ring-Down Spectroscopy analyser (CM-CRDS, with a G2101-i Analyzer,
18 209 Picarro, California, USA). Total POC and its $\delta^{13}\text{C}$ signature were determined with a precision of ± 0.3
19 210 ‰ at 250 μgC . Due to low POC loading of the filters, the $\delta^{13}\text{C}$ values below the 40m-depth sample
20 211 may be inaccurate and were deleted. The stable carbon isotope composition was calculated relative
21 212 to the international Vienna Pee Dee Belemnite standard.
22
23 213
24 214 HPLC-pigments
25
26 215 Samples for pigment analysis were collected through gentle filtering (<15 KPa) of two to four litre of
27 216 water over 4.5 cm Whatman GF/F filters. Filters were snap-frozen in liquid nitrogen, wrapped in
28 217 aluminium foil and stored at -80°C until analysis at the home laboratory. Before extraction in 90%
29 218 acetone, filters were freeze-dried at -55°C during 48 h (24). Pigments were analysed by high-
30 219 performance liquid chromatography on a Waters system equipped with a photodiode array (24) (25).
31 220 A Waters DeltaPak reversed-phase column (C18, fully end-capped) was used. Pigment standards
32 221 were obtained from DHI Water Quality Institute (Horsholm, Denmark).
33
34 222
35 223 Ancillary data
36
37 224 Several ancillary data were used to describe the chemistry across the cruise track. Sampling and
38 225 analyses of macro nutrients, the dissolved inorganic carbon system, oxygen isotopes of seawater and
39 226 parameters measured directly with a Seabird conductivity-temperature-depth (CTD) package
40 227 attached to the rosette frame (including oxygen, Chlorophyll *a* fluorescence, PAR) are described in
41 228 Henley et al. (23). Samples for determination of the stable isotopes of oxygen in seawater were
42 229 processed as described in Henley et al. (23), which also outlines their use for quantification of the
43 230 relative contributions of sea-ice melt and meteoric water to the freshwater content of the sample.
44 231 The mixed layer depth (MLD) is defined as the depth where the potential density exceeds that at the
45 232 surface by 0.05 kg m^{-3} , based on definitions in Venables et al. (15). □
46
47 233
48 234 *Data representation and statistical analyses*
49
50 235 All transect-distribution plots were done with Ocean Data View version 4.6.1 using weighted-average
51 236 gridding.
52
53 237 CHEMTAX matrix factorization was applied to derive algal classes from pigment patterns (26). The
54 238 initial pigment ratio included eight algal classes (Table 1). These classes were chosen based on
55 239 literature information (e.g.(27) (28)) and microscopy. Two groups of diatoms were described.
56 240 Diatoms_1 contained typical diatom species that are characterised by chlorophyll $c_{1,2}$ (Chl $c_{1,2}$).
57 241 Diatoms_2 is a separate group in which Chl c_1 is replaced by Chl c_3 . This group represents
58 242 *Pseudonitzschia* sp., though not exclusively. Haptophytes were also separated in two groups,

representing Haptophytes 6, 7, 8 as defined by Zapata et al.(29): Haptophyte-C represents amongst others Chrysomonadales; Haptophyte-P represents amongst others *Phaeocystis antarctica* (van Leeuwe et al 2014). Dinoflagellates were described as a separate class that was defined by peridinin. However, as many dinoflagellates do not carry peridinin, this group is probably underestimated. The input ratios were based on (30).

To establish significant effects of a number of biochemical factors on sulphur compounds, data of the top 25m were analysed by linear modelling in R (RStudio, 0.99.902). The models were tuned down to three variables; a number sufficiently adequate for data interpretation and with a relative high precision to improve model robustness. To this end, the Akaike Information Criteria was applied, which combines the goodness of fit to the number of parameters in the model, whilst defining hierarchy in the parameters (31). Canonical correspondence analysis (CCA) was performed in R (RStudio, 0.99.902, Vegan package) to evaluate the relationship between the community composition as calculated with CHEMTAX and abiotic parameters. Abiotic parameters included salinity, nitrate, silicate, phosphate, O₂, dissolved inorganic carbon (DIC) and the fractional contribution of sea-ice melt and meteoric water to the water composition.

Results

Hydrographic conditions:

The JR307 cruise took place under conditions of a retreating MIZ, with many small-sized ice floes present close to the sampling stations (Figure 2c). An extensive description of nutrient and carbon dynamics over the full water depth along the transect is provided in Henley et al. (23). The upper 120m is characterized by a relatively shallow mixed layer of <15m along the whole transect (Table 2). The pycnocline extends to depths varying between 25 and 40 m. A layer of cold Winter Water was persistently present between the pycnocline and 100-120 m depth. The largest signature of Circumpolar Deep Water (CDW) protruding into surface waters is seen closest to the coast at stations T09 and T10 where upwelling of relatively warm and saline water occurs (Fig. 2a, b).

Sea ice melt along the transect calculated from isotope mass balance techniques (e.g. (32), (33)) show fractions of -0.02 at around 60-80m depth up to +0.04 in the surface layers (Figure 2c). The presence of some negative values is not unexpected; the nature of the calculation produces positive values for waters that have been freshened by net sea-ice melt, and negative values for waters that have been salinified by brine rejection due to net sea ice production. The waters in the 60-80m layer correspond broadly with the Winter Water layer (i.e. the remnant of the previous winter's mixed layer), consistent with them showing the imprint of net sea ice production. Near the surface, the pattern of sea-ice melt is roughly inverse to that of salinity, indicating the impact of sea ice melt on the salinity distribution in this layer. The range of sea ice melt values is consistent with full-WAP surveys of $\delta^{18}\text{O}$ conducted across several years (33). Lowest contributions of sea-ice melt were observed in the innermost stations, with an increasing trend towards the shelf edge. An opposite trend was observed for the contribution of meteoric water to the surface-water composition.

Biomass and productivity indicators:

High levels of chlorophyll *a* (Chl *a*) characterised the surface waters, with an average concentration measured at 5 m of 5 $\mu\text{g/L}$ and a range of 1-7.5 $\mu\text{g/L}$ (Table 2). The highest concentrations were observed at stations T03, T05, T09 and CH1 (Figure 3a). Chl *a* data from the discrete HPLC analyses corresponded well with the *in situ* fluorescence measurements ($y = 1.0703x + 0.1355$, $R^2 = 0.9185$; data not shown), especially considering that the CTD-data are subject to variations due to daytime quenching of fluorescence (see Xing et al. for discussion (34)).

Particulate organic carbon (POC) displayed a similar pattern with average values of 600 $\mu\text{g/L}$, and maximum values of over 900 $\mu\text{g/L}$ in surface waters at stations T05 and T08 (Figure 3b). The stable isotope composition of POC indicated the enrichment of POC with the heavier ^{13}C -isotope at the

1
2 292 surface, except for station T02 (Figure 3c). High $\delta^{13}\text{C}$ -POC values appear to extend to deeper waters
3 293 at stations T01, T03, T05, T06 and all inner shelf stations.

4 294 Nutrient, oxygen and DIC profiles indicated net community production (Figure 4). Compared to
5 295 values below the euphotic zone, DIC in the upper mixed layer was reduced from 2220 $\mu\text{mol/kg}$ to
6 296 1950 $\mu\text{mol/kg}$, with pH increasing from 7.9 to 8.3 (Table 2 and Figure 4a), which resulted in a reduced
7 297 CO_2 concentration of 8-13 $\mu\text{mol/kg}$ (Figure 4b). Oxygen concentrations increased from a mean of
8 298 250-300 $\mu\text{mol/L}$ below the MLD to ~ 400 $\mu\text{mol/L}$ in surface waters, with large spatial variations (Table
9 299 2 and Figure 4c). Carbon reductions and oxygen supersaturations between 110 and 140% indicated a
10 300 productive surface community.

11
12 301 When considering half-saturation constants for nutrient uptake for diatoms of 0.24 μM for
13 302 phosphate and 1.6 μM for nitrate (35), primary production was potentially nitrate or phosphate-
14 303 limited at station T05 and to a lesser extent at stations T03 and T07 (Table 2 and Figure 4d).
15 304 Phosphate and silicic acid exhibited similar patterns as nitrate, but silicic acid remained above 45 μM
16 305 (see Henley et al. (23) for more detail on nutrient sources and sinks).

17
18 306

19 307 *Community composition:*

20
21 308 Based on HPLC-pigment fingerprints (of which several are given in Figures 5a-d), the phytoplankton
22 309 community composition was calculated with CHEMTAX software (26). Diatom contribution
23 310 decreased offshore from more than 50 % of the phytoplankton community at the innermost stations
24 311 to less than 25 % at the outermost stations (Figure 5e). An increasing contribution of both
25 312 Haptophyte types (characterized by 19'-hexanoyloxy-fucoxanthin and other pigments; Table 1, Figure
26 313 5c, e) was observed towards the outermost stations. Green algae, which contain chlorophyll *b* (Figure
27 314 5d), contributed around 20 % to total Chl *a*. This group was mainly represented by Chlorophytes;
28 315 Cryptophytes were only observed at stations T02 and T04 where the total Chl *a* inventory of the
29 316 surface 25 m water column was low (Figure 5f). Prasinophytes and dinoflagellates were only minor
30 317 contributors to the phytoplankton biomass, but might have been underestimated somewhat (see
31 318 Materials and Methods section).

32
33 319

34 320 *DMSP distribution:*

35
36 321 Distribution of both DMS(P)t and DMS(P)d exhibited similar patterns to other biological parameters
37 322 (Figure 6a, b). Very high DMS(P)t concentrations were observed in surface waters of stations T03 and
38 323 T05 through T08, with values between 565 and 640 nM and a lower but still high concentration of
39 324 429 nM at station T01 (Table 2). At 100 m depth DMS(P)t concentrations ranged between 1 and 8 nM.

40
41 325 On average, DMS(P)d contributed 25% (sd = $\pm 18\%$) to the total DMS(P)t concentration. Highest
42 326 concentrations were found at stations T03 and T06, with concentrations between 140 and 275 nM,
43 327 and slightly lower concentrations between 60 and 85 nM at stations T01, T04 and T05 (Table 2).
44 328 Concentrations at 100 m depth were between 0.8 and 1.5 nM. The high concentration of DMS(P)d at
45 329 station T06 did not coincide with any other outstanding parameter, except that the highest – but still
46 330 relatively low – concentration of zeaxanthin was observed at this station. Zeaxanthin is found in
47 331 specific types of dinoflagellates.

48
49 332

50 333 **Discussion**

51 334 *Phytoplankton community composition across the shelf*

52
53 335 A gradual shift in species composition was observed across the shelf, with diatoms dominating the
54 336 inner shelf area and an increasing importance of Haptophytes towards the outer shelf area. A strong
55 337 correlation between phytoplankton biomass and O_2 saturation, nitrate depletion and DIC drawdown
56 338 was observed, and indicated that the community had been growing healthily, with no trace-element

limitation of primary production evident in this shelf setting (Figure 7). This observation of an early summer-phytoplankton bloom is a common feature at the WAP (36) (37).

The ^{13}C -enrichment in surface samples along the cruise track was likely a reflection of high rates of growth and biological CO_2 uptake, as well as input of POC from sea ice. High $\delta^{13}\text{C}$ -POC values are often found in sea ice with high Chl *a* and POC concentrations, due to CO_2 uptake within the semi-closed sea ice matrix, where CO_2 exchange is limited so drawdown is intense (38) (39). In addition, ice melt can result in favourable growth conditions in the surface ocean by stabilising the upper water column, thereby providing an optimal light climate and potentially an input of micronutrients such as iron (40). Such conditions will also result in high $\delta^{13}\text{C}$ -values, as previously recorded in Ryder Bay (39), the Ross Sea (41) and Prydz Bay (42). No direct correlation could be observed between $\delta^{13}\text{C}$ -POC and the community structure, and we suggest that this is the result of mixed controls on $\delta^{13}\text{C}$ -POC imposed by sea ice inputs and variability in growth rates.

The CCA analysis indicated that the presence of Haptophytes-C could best be explained by the relatively strong component of sea-ice melt (Figure 7). The unique relationship between Haptophytes-C and sea-ice melt suggests that sea-ice has a role in enriching the pelagic algal community, as is often suggested but difficult to establish (17). Cryptophytes were only observed at the outer-shelf stations T02 and to a lesser extent at T04, where relatively low Chl *a* concentrations and low contributions of ice melt were observed. Cryptophytes have been linked with low salinity, colder water (43) (44) and more specifically with glacial melt (e.g. (45), but results from our CCA-analysis do not show these relationships (Figure 7).

The other groups distinguished by CHEMTAX were grouped more closely together. Especially the clustering of Haptophytes-P, representing amongst others *Phaeocystis antarctica*, and diatoms is remarkable. The two groups are often suggested to thrive in different habitats. In the Ross Sea it was observed that diatoms are more abundant under more stable light conditions, whereas Haptophytes are assumed to be better adapted to dynamic light conditions (46). However, a recent analysis of RaTS data (28) and Palmer LTER data (44) revealed a stable background population of flagellate species (Haptophytes and Cryptophytes), which is masked by high diatom abundances in high chlorophyll years. These findings are in agreement with our observations showing that Haptophytes are omnipresent. Whilst these groups contribute less to algal biomass, as a result of their smaller size, they are of high importance for DMS(P) fluxes.

Drivers of DMS(P) production

Sulphur compounds, POC and Chl *a* in the surface waters varied by a factor of 5 to 6 over the entire transect. When using a linear model to explain the drivers of the DMS(P) concentration, DMS(P)t and DMSPp were best explained by POC, then by the Haptophyte pigment Hex-Fuco and thirdly by the oxygen concentration. The DMS(P)d pool was best explained by the nitrate concentration, then POC and another Haptophyte pigment, Hex-kFuco (Table 3).

The fact that POC explains DMSPp better than the total phytoplankton biomass expressed as Chl *a* or the Haptophyte contribution to the community is intriguing and was examined further. A potential contributor to high POC loading of the water column is sea-ice melt. Upon ice melt, ice algae that contain DMSP are released to the upper water column. High concentrations of DMSP in the MIZ have been attributed to this process (e.g. (19) (18), but not studied in detail in the Antarctic. Compared to an Arctic study on sea ice and release of algal biomass and DMSP to the underlying water (47), our DMSP-to-Chl *a* ratios were very high (10 versus 64 ± 26.5 mmol DMSP g Chl a^{-1}), highlighting the difference in community structure. In the Arctic study an under-ice bloom of diatoms developed, whereas we found a substantial contribution of Haptophytes to the community. At the same time, the DMSPp-to-POC ratios in our samples were relatively low (514 ± 157 $\mu\text{mol DMSP g C}^{-1}$ or 0.006 ± 0.002 mol:mol). These values are substantially less than the 0.011 mol:mol observed in cultures of Haptophyte algae (22) and suggest additional sources of POC.

Sea ice contains different communities with very different DMSP-to-Chl a ratios. The well-known DMSP producer *Phaeocystis* sp. has often been found to dominate surface-ice communities, whereas the bottom-ice community mainly consists of large diatoms (20) (47) (17). DMSP-to-Chl a ratios in these communities can vary by up to an order of magnitude, with ratios between 200 and 500 in surface communities and less than 20 in bottom communities (20) (22). However, biomass accumulations in the bottom-ice communities are much higher than in the surface-ice community. Therefore, the melt of sea ice may have opposing impacts on the DMSP signature of the water column: a high POC loading can result in high DMSP concentrations, but low DMSP-to-Chl a ratios when containing mainly diatoms, whereas a low POC loading can also result in high DMSP and high ratios when containing mainly Haptophytes. These effects were also observed in the present study. High POC loading – which is associated with high Chl a – and high DMSP concentrations of surface waters were largely associated with sea-ice melt (Figure 8a), whereas high Chl a and lower DMSP concentrations often corresponded with lower sea-ice melt signatures (Figure 8b). The association of Haptophytes with elevated sea-ice melt (Figure 7 and 8c) indicate that the DMSP signature on the WAP shelf was driven by a combination of high POC loading and the contribution of Haptophytes, both of which were associated with sea ice melt. The surface value with second-highest sea-ice melt and relatively low DMSP concentration was observed at station T04, which exhibited very low Chl a levels. This may indicate a relatively recent input of sea-ice.

The inverse correlation between both the DMS(P)t pool and the DMSP pool (data not shown) versus salinity (R^2 of 0.685 and 0.662 respectively) provides further supporting evidence for the impact of sea-ice melt on the biogeochemical composition of the upper water column (Figure 8d). Sea-ice melt can also lead to increased DMSP through stabilization of the upper mixed layer and a subsequent increase in primary production as a result of favourable light conditions. Growth conditions did have a positive control on DMSP production (Table 3), but were of much less importance than the community composition and total organic biomass, both of which were influenced strongly by sea-ice melt. On the contrary, phytoplankton uses DMSP as an osmolyte and hence reduced concentrations are to be expected when algae have to adapt to lower salinities in an ice-melt event. The fact that the opposite is shown in the present study indicates the release of ice-associated algae with high concentrations of DMSP as the primary driver of the changes in DMSP that we observe. Whilst it could be expected that the release of intracellular DMSP – and conversion to DMS – would increase upon ice melt as ice algae are introduced to relatively fresh melt water, there was no correlation between DMS(P)d and salinity in the present study.

A more detailed investigation of the phytoplankton-pigment fingerprint also showed a correlation between DMS(P)t and DMS(P)d with zeaxanthin (data not shown). This suggests a contribution of dinoflagellates to both the production and conversion of DMSP, although the contribution of this group to total Chl a was minor. Both Haptophytes and dinoflagellates are well known for their extremely high intracellular DMSP concentrations and expression of enzymes that convert DMSP to DMS (48) (22). The presence of algal DMSP-lyases can result in high fractional DMS production from dissolved DMSP, whereas bacterial conversion of DMSPd often follows the demethylation pathway, which does not yield DMS (22) (49). Although the highest concentrations of DMS(P)d were indeed observed at stations with high zeaxanthin and hex-fuco, the fractional contribution to DMS(P)t was not particularly high. For example, only the surface samples of stations T04 and T06 contained a slightly higher than average contribution of DMS(P)d, 38 and 48 % respectively. Since both Haptophytes and dinoflagellates appeared to co-occur, distinguishing the contribution of each group to DMSPd is difficult to achieve.

Implications for the WAP

The objective of this study was to obtain a better understanding of the ecological parameters that drive the pronounced heterogeneity in DMS(P) dynamics and to study the relative contribution of DMS(P) released from sea ice to the pelagic environment. All biogeochemical parameters were highly variable along the cross-shelf transect and a clear signature of sea-ice melt could be detected in the

DMS(P) distribution. Gali et al. (50) made a first attempt to produce a global DMSPt climatology. The authors used a global database of DMSP and ancillary measurements to create a remote sensing algorithm for phytoplanktonic DMSP. Available data of DMSPt and Chl *a* were binned into Longhurst provinces and seasonal means. For the Austral Polar province (APLR) in spring, they calculated approximately 50 nM DMSPt and 2 µg/L chl-*a*, whilst summer values of 110 nM DMSPt and 0.5 µg/L Chl *a* and autumn values of 100nM DMSPt and 3 µg/L Chl *a* were obtained ((50), suppl. mat. figure S2). In our study, DMS(P)t values in surface waters ranged between 94 and 643 nM (average 398 nM) and DMSPP ranged between 76 and 572 nM (average 323 nM), which is considerably higher than the climatological value for the APLR (50).

The DMS(P)d concentrations provide an upper limit to the potential concentration of DMS. Taking a conservative estimate of 80 % DMS in the JR307 DMS(P)d samples, this means that DMS concentrations ranged mostly between 30 and 220 nM, except for stations T02, T09 and CH1 where concentrations were between 10 and 15 nM. These concentrations are well above the current DMS climatology for the WAP region, which provides a summer-time value of around 10 nM (9), suggesting that DMS fluxes along the WAP shelf may be significantly higher than previously estimated. In the adjacent Ryder Bay, similar values for DMS concentration were observed in the 2014/15 season (Webb et al. in prep.). Although this season showed the highest values in our five-year time series from Ryder Bay, summertime DMS concentrations exceeded 30 nM during four out of the five years (Webb et al. in prep.).

Both the DMSP and the DMS climatologies do not account for the large and dynamic fluctuations we observed during our one-week sampling of the WAP shelf. The strong sea-ice signal we observed indicates that the contribution of the Antarctic coastal zone to the production of DMS(P) depends strongly on the sea-ice distribution. With a potential further reduction of sea ice along the WAP, this may lead to reductions of DMS(P) production with implications for feedback processes on regional and larger-scale climate system processes.

Acknowledgements:

We are grateful to the captain and crew of RRS James Clark Ross for their support during the cruise. We thank Ronald Visser for pigment analysis and Laura Gerrish and Louise Ireland for providing the sea-ice coverage graphs. JS, MAVL and ALW were funded through the Dutch Science Foundation (NWO) under the Polar Program, project numbers 866.10.101 and 866.14.101. EMJ was funded through project 866.13.006 under the Netherlands Polar program at NWO. SFH and the JR307 cruise were funded by the UK Natural Environment Research Council (NERC) through an independent research fellowship (NE/K010034/1) and the British Antarctic Survey's Polar Oceans program.

References:

1. Gondwe M, Krol M, Gieskes W, Klaassen W, de Baar H. The contribution of ocean-leaving DMS to the global atmospheric burdens of DMS, MSA, SO₂, and NSS SO₄ =. *Global Biogeochem Cycles* [Internet]. 2003;17(2):25–1. Available from: <http://adsabs.harvard.edu/abs/2003GBioC...17b..25G>
2. Charlson RJ, Lovelock JE, Andreae MO, Warren SG. Oceanic phytoplankton, atmospheric sulphur, cloud albedo and climate. *Nature* [Internet]. 1987;326(6114):655–61. Available from: <http://www.nature.com/doi/10.1038/326655a0>
3. Von Glasow R. A look at the CLAW hypothesis from an atmospheric chemistry point of view. *Environ Chem*. 2007;4(6):379–81.
4. Humphries RS, Klekociuk AR, Schofield R, Keywood M, Ward J, Wilson SR. Unexpectedly high ultrafine aerosol concentrations above East Antarctic sea ice. *Atmos Chem Phys*. 2016;16(4):2185–206.
5. Zemmeling HJ, Houghton L, Dacey JWH, Stefels J, Koch BP, Schröder M, et al. Stratification and the distribution of phytoplankton, nutrients, inorganic carbon, and sulfur in the surface waters of Weddell Sea leads. *Deep Res Part II Top Stud Oceanogr*. 2008;55(8–9):988–99.
6. Zemmeling HJ, Dacey JWH, Houghton L, Hintsa EJ, Liss PS. Dimethylsulfide emissions over the multi-year ice of the western Weddell Sea. *Geophys Res Lett*. 2008;35(6):4–7.
7. Cameron-Smith P, Elliott S, Maltrud M, Erickson D, Wingenter O. Changes in dimethyl sulfide oceanic distribution due to climate change. *Geophys Res Lett*. 2011;38(7):1–5.
8. Lana A, Bell TG, Simó R, Vallina SM, Ballabrera-Poy J, Kettle AJ, et al. An updated climatology of surface dimethylsulfide concentrations and emission fluxes in the global ocean. *Global Biogeochem Cycles*. 2011;25(1):1–17.
9. Jarníková T, Tortell PD. Towards a revised climatology of summertime dimethylsulfide concentrations and sea-air fluxes in the Southern Ocean. *Environ Chem*. 2016;13(2):364–78.
10. Herrmann M, Najjar RG, Neeley AR, Vila-Costa M, Dacey JWH, DiTullio GR, et al. Diagnostic modeling of dimethylsulfide production in coastal water west of the Antarctic Peninsula. *Cont Shelf Res*. 2012;32:96–109.
11. Asher EC, Dacey JWH, Stukel M, Long MC, Tortell PD. Processes driving seasonal variability in DMS, DMSP, and DMSO concentrations and turnover in coastal Antarctic waters. *Limnol Oceanogr*. 2017;62(1):104–24.
12. Stammerjohn S, Massom R, Rind D, Martinson D. Regions of rapid sea ice change: An inter-hemispheric seasonal comparison. *Geophys Res Lett*. 2012;39(6):1–8.
13. Ducklow H, Fraser W, Meredith M, Stammerjohn S, Doney S, Martinson D, et al. West Antarctic Peninsula: An Ice-Dependent Coastal Marine Ecosystem in Transition. *Oceanography* [Internet]. 2013;26(3):190–203. Available from: <http://www.tos.org/oceanography/archive/26->

- 3_ducklow.html%5Cnhttp://tos.org/oceanography/article/west-antarctic-peninsula-an-ice-dependent-coastal-marine-ecosystemintransit
14. Montes-Hugo M, Martinson DG, Stammerjohn SE, Schofield OM. Recent Changes in Phytoplankton Western Antarctic Peninsula. *Science* (80-). 2009;323(March).
 15. Venables HJ, Clarke A, Meredith MP. Wintertime controls on summer stratification and productivity at the western Antarctic Peninsula. *Limnol Oceanogr* [Internet]. 2013;58(3):1035–47. Available from: <http://doi.wiley.com/10.4319/lo.2013.58.3.1035>
 16. Thomas DN, Dieckmann GS. Antarctic Sea ice--a habitat for extremophiles. *Science* (80-). 2002;295(5555):641–4.
 17. van Leeuwe MA, Tedesco L, Arrigo KR, Assmy P, Campbell K, Meiners KM, et al. Microalgal community structure and primary production in Arctic and Antarctic sea ice: A synthesis. *Elem Sci Anth* [Internet]. 2018;6. Available from: <http://www.elementascience.org/articles/10.1525/elementa.267/>
 18. Trevena AJ, Jones GB. Dimethylsulphide and dimethylsulphoniopropionate in Antarctic sea ice and their release during sea ice melting. *Mar Chem*. 2006;98:210–22.
 19. Kirst GO, Thiel C, Wolff H, Nothnagel J, Wanzek M, Ulmke R. Dimethylsulfoniopropionate (DMSP) in icealgae and its possible biological role. *Mar Chem*. 1991 Nov;35:381–8.
 20. Tison JL, Brabant F, Dumont I, Stefels J. High-resolution dimethyl sulfide and dimethylsulfoniopropionate time series profiles in decaying summer first-year sea ice at Ice Station Polarstern, western Weddell Sea, Antarctica. *J Geophys Res Biogeosciences*. 2010;115(4):1–16.
 21. Asher EC, Dacey JWH, Mills MM, Arrigo KR, Tortell PD. High concentrations and turnover rates of DMS, DMSP and DMSO in Antarctic sea ice. *Geophys Res Lett*. 2011;38(23):1–5.
 22. Stefels J, Steinke M, Turner S, Malin G, Belviso S. Environmental constraints on the production and removal of the climatically active gas dimethylsulphide (DMS) and implications for ecosystem modelling. *Biogeochemistry*. 2007;83:245–75.
 23. Henley SF, Jones EM, Venables HJ, Meredith MP, Firing YL, Dittrich R, et al. Macronutrient and carbon supply, uptake and cycling across the Antarctic Peninsula shelf during summer. *Philos Trans A*. 2018;
 24. van Leeuwe MA, Villerius LA, Roggeveld J, Visser RJW, Stefels J. An optimized method for automated analysis of algal pigments by HPLC. *Mar Chem*. 2006;102(3–4):267–75.
 25. Heukelem L Van, Thomas CS. Computer-assisted high-performance liquid chromatography method development with applications to the isolation and analysis of phytoplankton pigments. *J Chromatogr*. 2001;910:31–49.
 26. Wright SW, Thomas DP, Marchant HJ, Higgins HW, Mackey MD, Mackey DJ. Analysis of phytoplankton of the Australian sector of the Southern Ocean: Comparisons of microscopy and size frequency data with interpretations of pigment HPLC data using the “CHEMTAX” matrix factorisation program. *Mar Ecol Prog Ser*. 1996;144(1–3):285–98.
 27. van Leeuwe MA, Kattner G, van Oijen T, de Jong JTM, de Baar HJW. Phytoplankton and pigment patterns across frontal zones in the Atlantic sector of the Southern Ocean. *Mar Chem* [Internet]. 2015;177:510–7. Available from: <http://dx.doi.org/10.1016/j.marchem.2015.08.003>
 28. Rozema PD, Venables HJ, van de Poll WH, Clarke A, Meredith MP, Buma AGJ. Interannual variability in phytoplankton biomass and species composition in northern Marguerite Bay (West Antarctic Peninsula) is governed by both winter sea ice cover and summer stratification. *Limnol Oceanogr*. 2017;62(1):235–52.
 29. Zapata M, Jeffrey SW, Wright SW, Rodríguez F, Garrido JL, Clementson L. Photosynthetic

- 558 pigments in 37 species (65 strains) of Haptophyta: Implications for oceanography and
559 chemotaxonomy. *Mar Ecol Prog Ser.* 2004;270:83–102.
- 560 30. Wright SW, van den Enden RL, Pearce I, Davidson AT, Scott FJ, Westwood KJ. Phytoplankton
561 community structure and stocks in the Southern Ocean (30–80°E) determined by CHEMTAX
562 analysis of HPLC pigment signatures. *Deep Res Part II Top Stud Oceanogr* [Internet].
563 2010;57(9–10):758–78. Available from: <http://dx.doi.org/10.1016/j.dsr2.2009.06.015>
- 564 31. Zuur AF, Ieno EN, Smith GM. Analyzing Ecological Data. Gail M, Krickeberg K, Sarnet J, Tsiatis A,
565 editors. *Methods.* NY: Springer; 2007. 672 p.
- 566 32. Meredith MP, Venables HJ, Clarke A, Ducklow HW, Erickson M, Leng MJ, et al. The freshwater
567 system west of the Antarctic peninsula: Spatial and temporal changes. *J Clim.*
568 2013;26(5):1669–84.
- 569 33. Meredith MP, Stammerjohn SE, Venables HJ, Ducklow HW, Martinson DG, Iannuzzi RA, et al.
570 Changing distributions of sea ice melt and meteoric water west of the Antarctic Peninsula.
571 *Deep Res Part II Top Stud Oceanogr* [Internet]. 2017;139:40–57. Available from:
572 <http://dx.doi.org/10.1016/j.dsr2.2016.04.019>
- 573 34. Xing X, Claustre H, Blain S, D’Ortenzio F, Antoine D, Ras J, et al. Quenching correction for in
574 vivo chlorophyll fluorescence acquired by autonomous platforms: A case study with
575 instrumented elephant seals in the Kerguelen region (Southern Ocean). *Limnol Oceanogr*
576 *Methods.* 2012;10(JULY):483–95.
- 577 35. Sarthou G, Timmermans KR, Blain S, Tréguer P. Growth physiology and fate of diatoms in the
578 ocean: A review. *J Sea Res.* 2005;53(1–2):25–42.
- 579 36. Clarke A, Meredith MP, Wallace MI, Brandon MA, Thomas DN. Seasonal and interannual
580 variability in temperature, chlorophyll and macronutrients in northern Marguerite Bay,
581 Antarctica. *Deep Res Part II Top Stud Oceanogr.* 2008;55(18–19):1988–2006.
- 582 37. Annett AL, Carson DS, Crosta X, Clarke A, Ganeshram RS. Seasonal progression of diatom
583 assemblages in surface waters of Ryder Bay, Antarctica. *Polar Biol.* 2010;33:13–29.
- 584 38. Fischer G. Stable carbon isotope ratios of plankton carbon and sinking organic matter from
585 the Atlantic sector of the Southern Ocean. *Mar Chem* [Internet]. 1991;35(1–4):581–96.
586 Available from: [http://dx.doi.org/10.1016/S0304-4203\(09\)90044-5](http://dx.doi.org/10.1016/S0304-4203(09)90044-5)
- 587 39. Henley SF, Annett AL, Ganeshram RS, Carson DS, Weston K, Crosta X, et al. Factors influencing
588 the stable carbon isotopic composition of suspended and sinking organic matter in the coastal
589 Antarctic sea ice environment. *Biogeosciences.* 2012;9(3):1137–57.
- 590 40. Lannuzel D, Schoemann V, De Jong J, Pasquer B, Van Der Merwe P, Masson F, et al.
591 Distribution of dissolved iron in Antarctic sea ice: Spatial, seasonal, and inter-annual variability.
592 *J Geophys Res Biogeosciences.* 2010;115(3):1–13.
- 593 41. Villinski JC, Dunbar RB, Mucciarone D a. Carbon 13 / Carbon 12 ratios of sedimentary organic
594 matter from the Ross Sea , Antarctica : A record of phytoplankton bloom dynamics The
595 carbon isotopic composition of phytoplankton input from sea ice communities enriched
596 increased heterotrophic these fac. *J Geophys Res.* 2000;105.
- 597 42. Zhang R, Zheng M, Chen M, Ma Q, Cao J, Qiu Y. An isotopic perspective on the correlation of
598 surface ocean carbon dynamics and sea ice melting in Prydz Bay (Antarctica) during austral
599 summer. *Deep Res Part I Oceanogr Res Pap* [Internet]. 2014;83:24–33. Available from:
600 <http://dx.doi.org/10.1016/j.dsr.2013.08.006>
- 601 43. Saba GK, Fraser WR, Saba VS, Iannuzzi RA, Coleman KE, Doney SC, et al. Winter and spring
602 controls on the summer food web of the coastal West Antarctic Peninsula. *Nat Commun*
603 [Internet]. 2014;5:1–8. Available from: <http://dx.doi.org/10.1038/ncomms5318>
- 604 44. Schofield O, Saba G, Coleman K, Carvalho F, Couto N, Ducklow H, et al. Decadal variability in

- coastal phytoplankton community composition in a changing West Antarctic Peninsula. *Deep Res Part I Oceanogr Res Pap.* 2017;124(November 2015):42–54.
45. Moline MA, Claustre H, Frazer TK, Schofield O, Vernet M. Alteration of the food web along the Antarctic Peninsula in response to a regional warming trend. *Glob Chang Biol.* 2004;10(12):1973–80.
46. Arrigo KR, Robinson DH, Worthen DL, Dunbar RB, DiTullio, G R, VanWoert M, Lizotte MP. Phytoplankton community structure and the drawdown of nutrients and CO₂ in the Southern Ocean. *Science* (80-). 1999;283:365–7.
47. Galindo V, Levasseur M, Mundy CJ, Gosselin M, Tremblay J-E, Scarratt M, et al. Biological and physical processes influencing sea ice, under-ice algae, and dimethylsulfoniopropionate during spring in the Canadian Arctic Archipelago. *J Geophys Res Ocean.* 2014;119:3746–66.
48. Caruana AMN, Malin G. The variability in DMSP content and DMSP lyase activity in marine dinoflagellates. *Prog Oceanogr* [Internet]. 2014;120:410–24. Available from: <http://dx.doi.org/10.1016/j.pocean.2013.10.014>
49. Johnston AWB, Green RT, Todd JD. Enzymatic breakage of dimethylsulfoniopropionate - a signature molecule for life at sea. *Curr Opin Chem Biol* [Internet]. 2016;31(Figure 1):58–65. Available from: <http://dx.doi.org/10.1016/j.cbpa.2016.01.011>
50. Galí M, Devred E, Levasseur M, Royer SJ, Babin M. A remote sensing algorithm for planktonic dimethylsulfoniopropionate (DMSP) and an analysis of global patterns. *Remote Sens Environ* [Internet]. 2015;171(November):171–84. Available from: <http://dx.doi.org/10.1016/j.rse.2015.10.012>

628 Table 1. Final optimized pigment ratios (pigment : Chl *a*) after CHEMTAX-analyses.

	Chl <i>c</i> ₂	Chl <i>c</i> ₃	Peri	Fuco	Neo	19'-Hexfuco	Allo	Chl <i>b</i>
Prasinophytes_1	0	0	0	0	0.073	0	0	0.687
Dinoflagellates	0	0	0.300	0	0	0	0	0
Cryptophytes	0.130	0	0	0	0	0	0.839	0
Haptophytes_P	0.337	0.293	0	0.201	0	0	0	0
Haptophytes_C	0.355	0.053	0	0.073	0	1.241	0	0
Chlorophytes	0	0	0	0	0.005	0	0	0.005
Diatoms_1	0.483	0	0	0.603	0	0	0	0
Diatoms_2	0	0.045	0	1.298	0	0	0	0

629 Abbreviations: Chl: chlorophyll; Peri: peridinin; Fuco: fucoxanthin; 19'-Hexfuco:
630 19'-hexanoyloxyfucoxanthin; Allo: alloxanthin.

631
632

633 Table 2. Mixed Layer Depth (MLD) and main characteristic biochemical parameters at 5-m depth for
634 each station along the JR307 cruise track. Stations are ordered from the shelf edge (T01) towards the
635 innermost station in Ryder Bay (T10).

station	MLD	salinity	CTD O ₂	nitrate	silicate	phosphate	DIC	alkalinity	pH	Chl <i>a</i>	POC	DMS(P)t	DMS(P)d
	m		μmol/L	μmol/L	μmol/L	μmol/L	μmol/kg	μmol/kg		μg/L	mg/L	nmol/L	nmol/L
T01	5	33.05	412.9	14.1	46.4	1.03	2041.0	2254.9	8.31	5.20	0.501	429	85
T02	9	33.27	357.8	22.6	55.0	1.54	2120.7	2262.8	8.13	1.12	0.222	94	18
T03	5	32.68	446.0	2.1	47.7	0.31	1978.2	2242.2	8.43	7.10	0.625	643	143
T04	9	32.55	393.3	14.8	50.0	1.04	2044.8	2222.0	8.25	3.23	0.351	221	85
T05	13	32.98	449.6	0.8	44.5	0.14	1959.1	2266.8	8.48	6.90	0.920	588	61
T06	3	33.08	399.9	7.4	49.1	0.58	2047.0	2241.7	8.27	5.22	0.615	580	275
T07	7	32.01	469.7	4.2	47.7	0.41	1953.2	2172.1	8.36	5.99	0.826	565	50
T08	7	33.06	431.9	5.5	45.4	0.44	2016.3	2272.3	8.39	4.55	0.930	609	36
CH1	5	33.33	422.6	11.1	53.3	0.80	2068.1	2277.7	8.29	7.51	0.725	267	13
T09	7	33.25	496.3	10.7	49.7	0.63	2066.6	2286.1	8.30	7.41	0.619	180	12
T10	7	33.42	364.0	21.1	60.0	1.51	2146.7	2281.3	8.12	2.81	0.308	202	46

636
637

638 Table 3. Significance levels derived by linear modelling for impact of POC, O₂, nitrate, Hex-Fuco and
639 Hex-kFuco on sulphur compounds. See text for abbreviations. n.d. = not determined

Sulfur compound	POC	O ₂	Nitrate	Hex-Fuco	Hex-kFuco
DMS(P)t	p < 1.03 e-08	p < 0.0177	n.d.	p < 1.00 e-07	n.d.
DMSPP	p < 5.92e-12	p < 0.00294	n.d.	p < 3.74e-06	n.d.
DMS(P)d	p < 0.000231	n.d.	p < 0.000131	n.d.	p < 0.000751

640
641

Figure captions:

Figure 1. Sea-ice concentration at the Western Antarctic Peninsula: Average concentration in October-November over the period 2013-2017 (A); Average concentration in December-January over the period 2013-2018 (B); Map of the study area showing the average sea-ice coverage just preceding the JR307 cruise (16-31 December 2014), and the eleven sampling stations (C).

Figure 2. Hydrographic conditions of the surface waters along the JR307 cruise track: a) potential temperature; b) salinity; c) fractional contribution of sea-ice melt to the surface water composition.

Figure 3. Spatial distribution of biological parameters along the JR307 cruise track. a) Chl *a* (in $\mu\text{g/L}$); b) particulate organic carbon (in mg/L); c) ^{13}C -isotopic signature of POC. Note different depth scales in c.: data below 40m depth were capped as they may be unreliable due to low POC loading of the samples.

Figure 4. Patterns of surface-water chemistry along the JR307 cruise track: a) pH; b) CO_2 concentration calculated from DIC and pH measurements; c) oxygen concentration as measured with the CTD sensor; d) nitrate concentration (from (23))

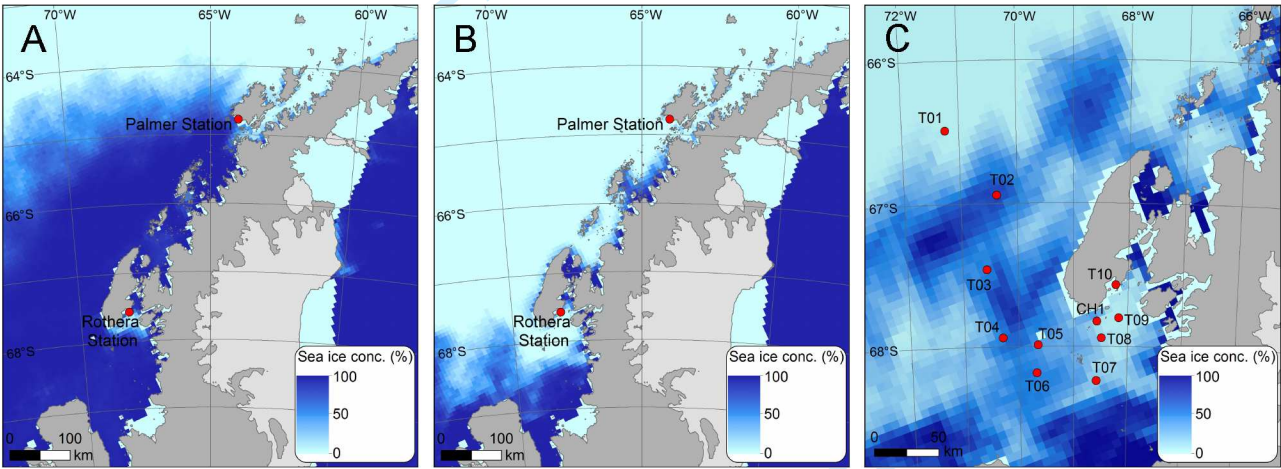
Figure 5. Phytoplankton pigment distribution along the JR307 cruise track. a) Chl *a* as in figure 3, for comparison; b) Fucoxanthin; c) 19'-hexanoyloxy-fucoxanthin; d) Chlorophyll-b; e) species contribution as percentage of total Chl *a* as calculated with CHEMTAX; f) absolute species contribution to the total Chl *a* burden of the upper 25 m, as calculated with CHEMTAX. All data in figures a) through d) in $\mu\text{g pigment/L}$.

Figure 6. Spatial distribution of DMS(P)t (a) and DMS(P)d (b) along the JR307 cruise track.

Figure 7. Ordination plot of a CCA analyses of species composition and abiotic parameters. The first two axes explain 92% of the variance. Sea-ice melt, nitrate and DIC concentration and O_2 -saturation are the strongest drivers (blue arrows) of algal species composition (in red), with a less differentiating role for glacial melt. The green circle clusters 5m surface samples. Deeper waters (15m and 25m) are distinguished in two more clusters: the black circle (1st quadrant) clusters coastal stations (T05 –T10) and the blue circle (2nd quadrant) shelf stations (T02 –T04). Numbers denote station ID and depth.

Figure 8. Correlations of the full data set between DMSPp and POC (a), DMSPp and Chl *a* (b), DMSPp and the Haptophyte pigment Hex-kFuco (c), and between the total DMS(P)t pool and salinity (d). The colour coding shows the fractional contribution of sea-ice melt to the water composition.

1
2
3
4
5
6
7
8
9
10
11
12
13
14
15
16
17
18
19
20
21
22
23
24
25
26
27
28
29
30
31
32
33
34
35
36
37
38
39
40
41
42
43
44
45
46
47
48
49
50
51
52
53
54
55
56
57
58
59
60



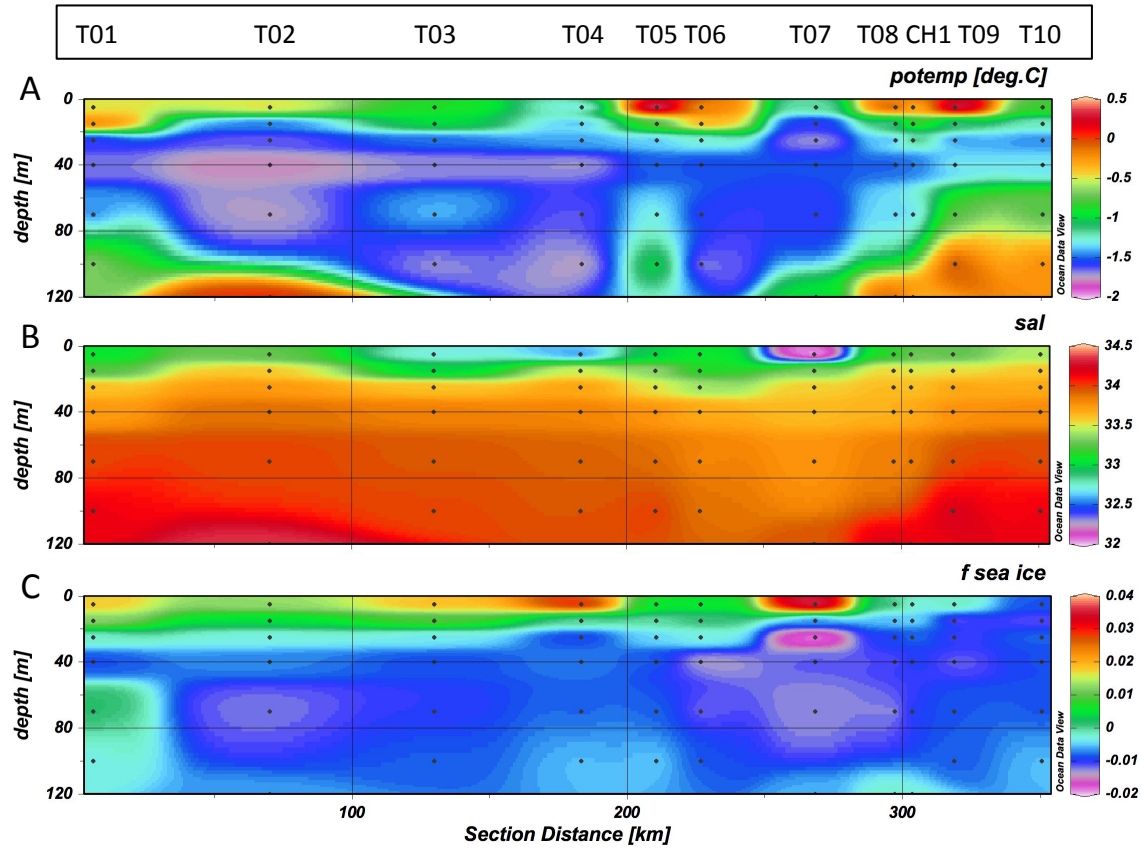


Figure 2.

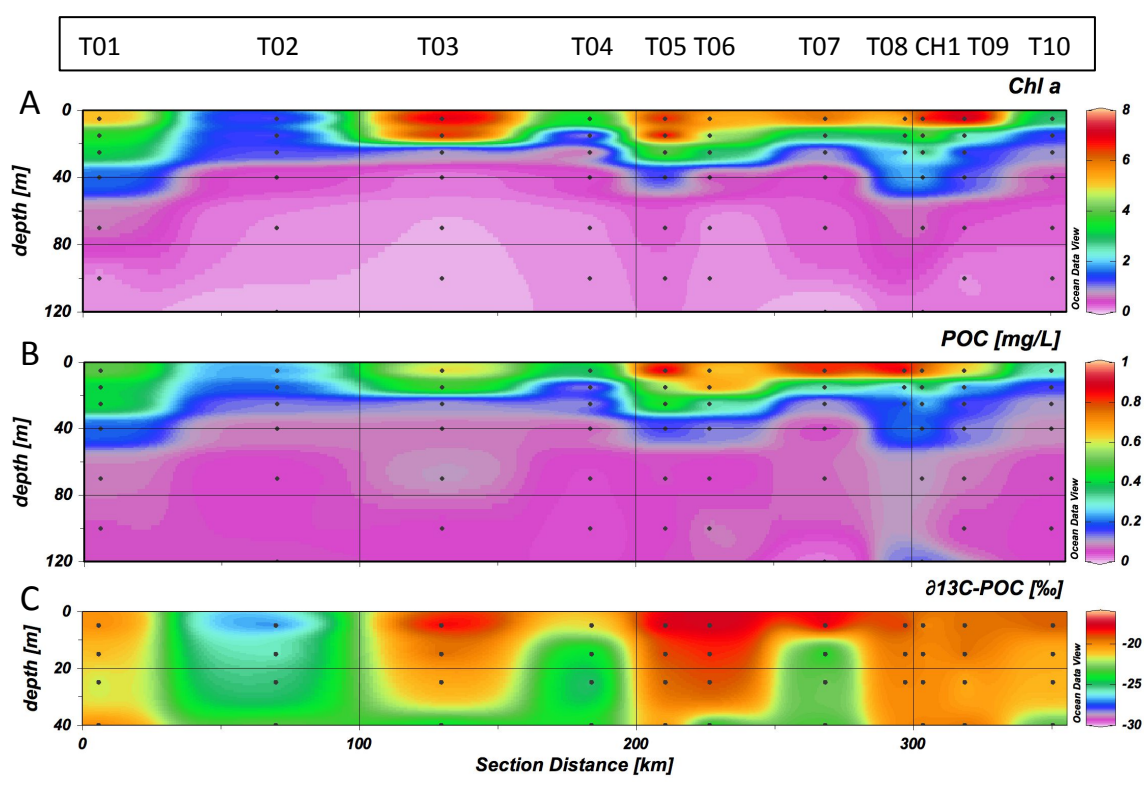


Figure 3.

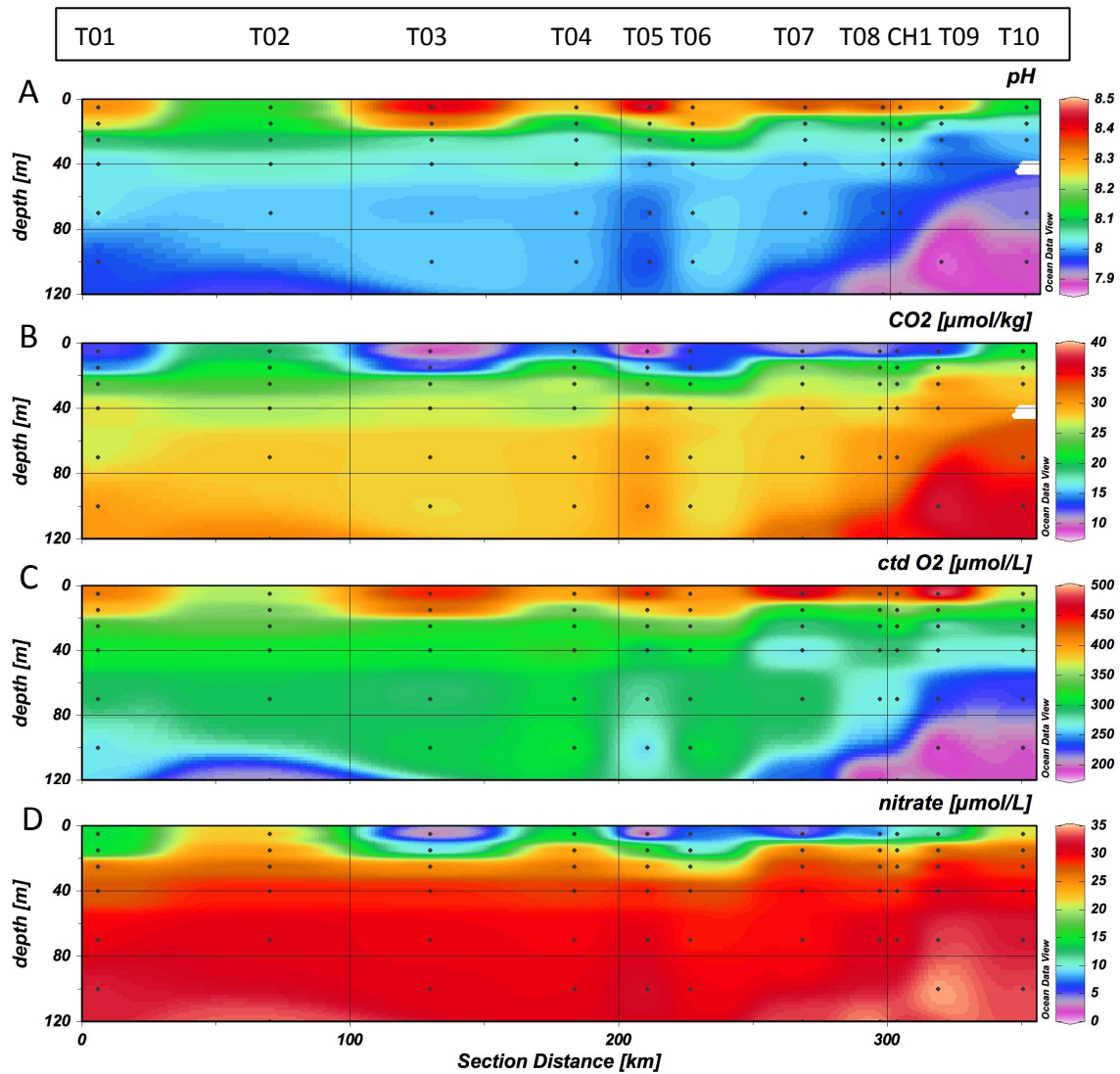


Figure 4.

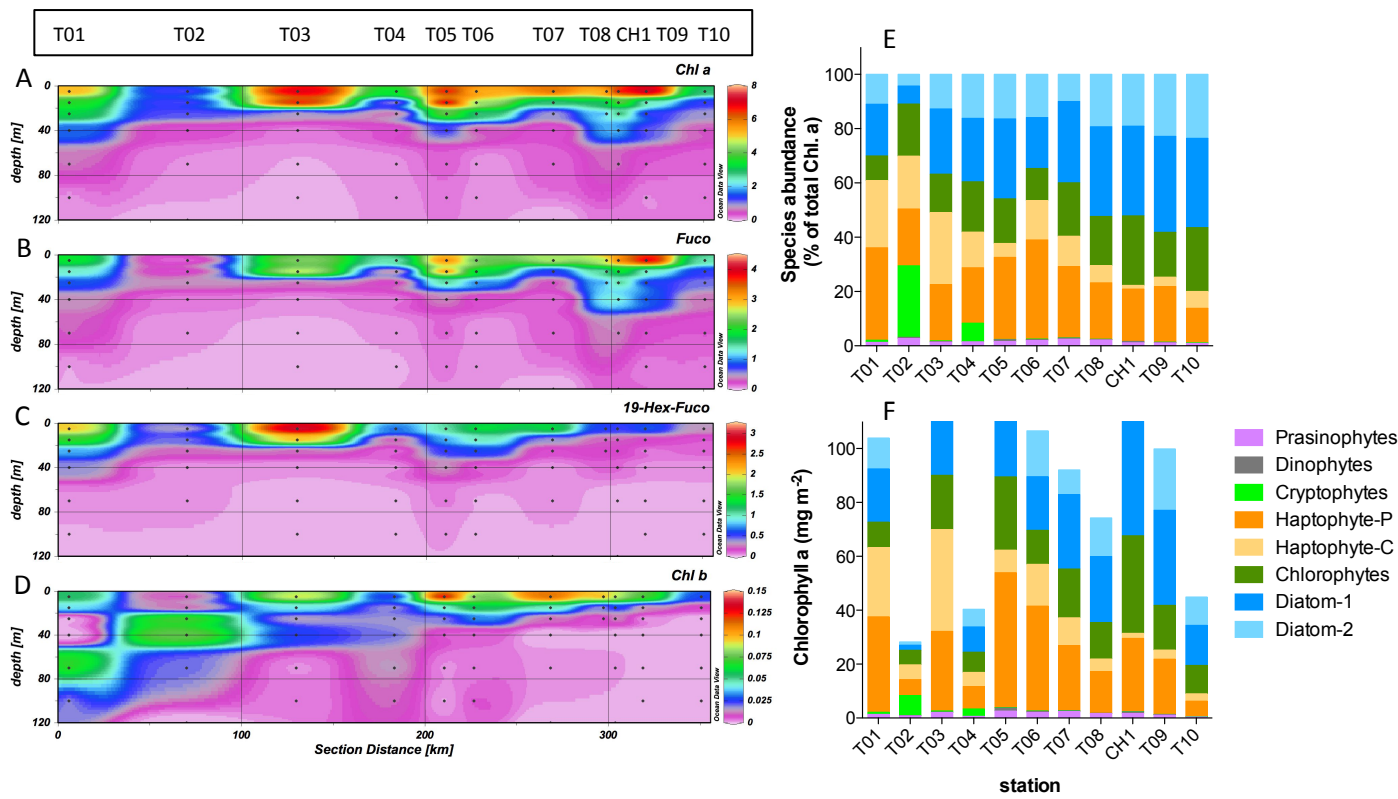


Figure 5.

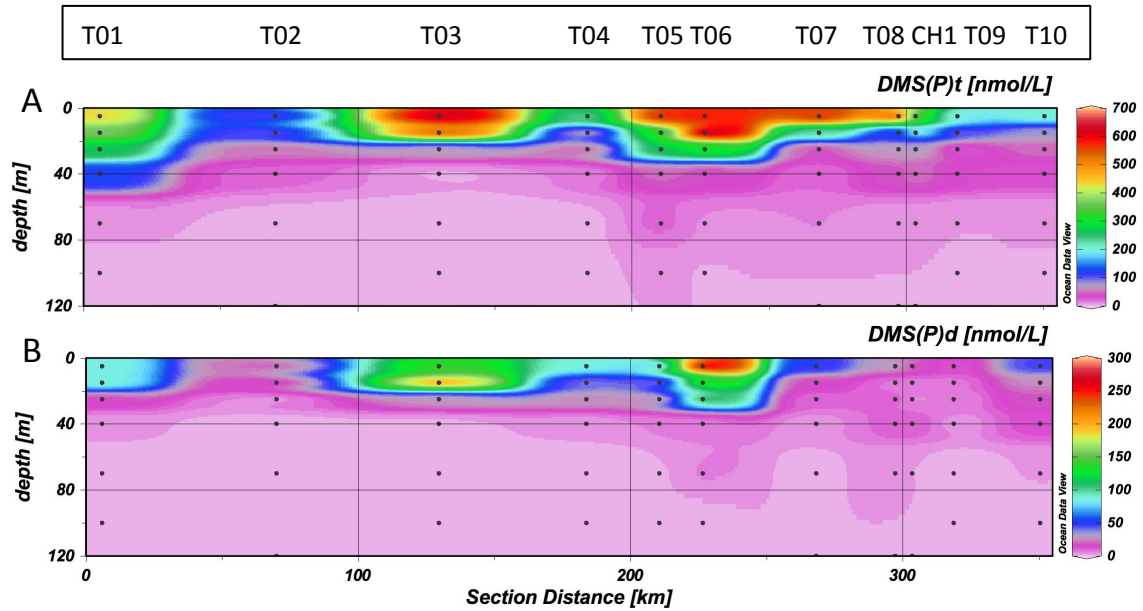
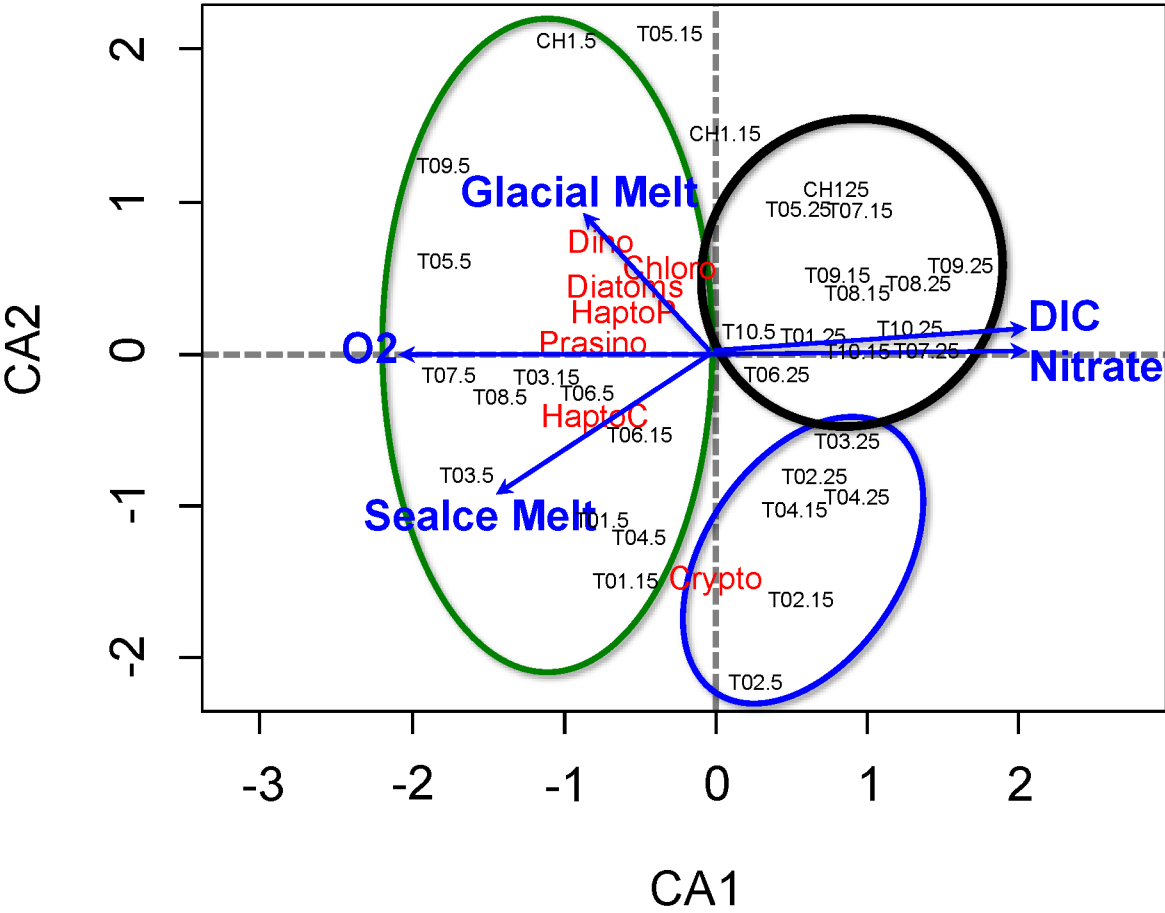
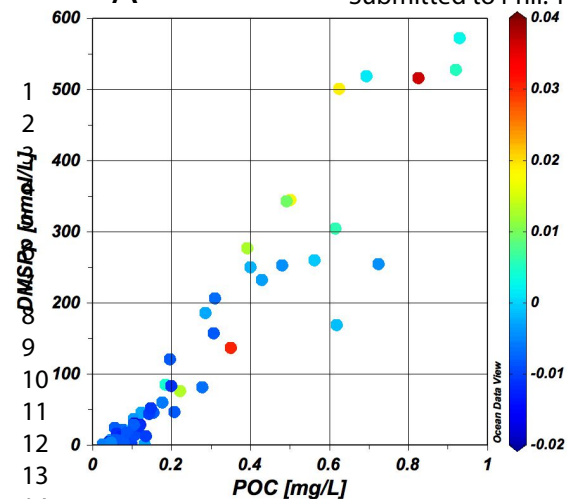


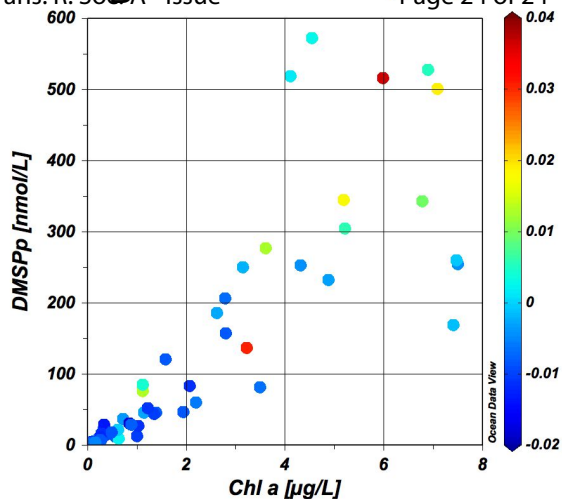
Figure 6.



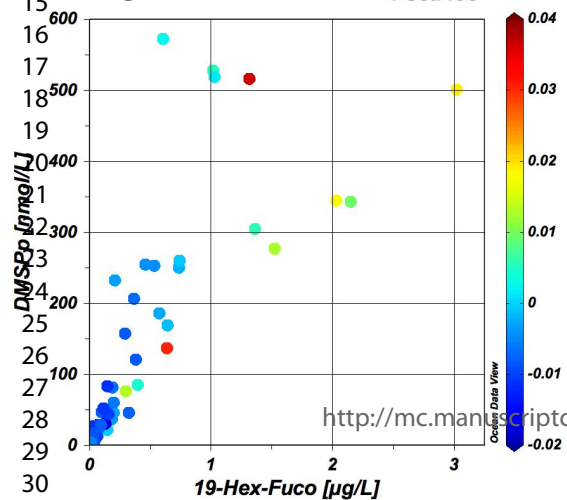
A



B



C



D

